Measurement Science and Technology

A time-domain ultrasonic approach for oil film thickness measurement with improved resolution and range

To cite this article before publication: Pan Dou *et al* 2020 *Meas. Sci. Technol.* in press https://doi.org/10.1088/1361-6501/ab7a69

A time-domain ultrasonic approach for oil film thickness measurement with improved resolution and range

Pan Dou[a], Tonghai Wu[a]* , Zhongxiao Peng[b]

[a] *Key Laboratory of Education Ministry for Modern Design and Rotor-Bearing System, Xi'an Jiaotong University, Xi'an, Shaanxi 710049, P.R. China*
[b] *School of Mechanical and Manufacturing Engineering, The University of New South Wales, Sydney, 2052, Australia*

*Corresponding author: wt-h@163.com

Abstract

Ultrasonic-based method has been proved to be a practical technique for measuring oil film thickness in an enclosed tribo-pair of a supporting bearing and under a dynamic condition. To cope with large-scale variations of the oil film thickness in engineering applications, frequency-domain based models, being adaptive for different measurement ranges, are widely used. As the improvement, time-domain approach can further expand the effective range, but it suffers a decreased resolution in oil thickness measurement. To address these issues, this paper proposed a unified time-domain model for full-range measurement. First, a cluster of standard echoes with definite film thicknesses in a wide range are pre-constructed, and they are matched with the measured echoes to find the most suitable oil film thickness. Further, an optimized interpolation was applied to both the constructed and the measured echoes for better resolution. Aiming at the lowest interpolation error, the windowed sinc function was employed optimally. Using a precision calibration rig, the proposed model was compared with the traditional frequency-domain and the time-domain models. The comparison has demonstrated that the proposed model has a larger effective measurement range covering those of all traditional frequency-domain models and with the equal accuracies. Meanwhile, the proposed model shows both a wider effective range and a higher resolution than that of the referred time-domain model. This work contributes to development of on-line, continuous measurement of oil film thickness varying in a large scale.

Keywords ─ Ultrasonic measurement; lubricant film thickness; Time-domain approach; Improvement of resolution

1. Introduction

It has been widely recognized that a thin lubricant layer plays an important role in all dynamic lubrication bearings, not only for load supporting but also for friction and wear resistance. Therefore, the lubricant film thickness is no doubt one of the most critical index for identifying the lubrication conditions of a bearing. However, it remains a difficult task to measure the ultra-thin oil film thickness of a running bearing. Any destructive method, e.g. an optical method which requires dismantling a bearing, is excluded, while indirect methods, e.g. the popular eddy current principle [1], may be able to estimate the average thickness between the tribopairs but lack of the distributed information. Furthermore, oil film thickness is often influenced by operating conditions, and therefore can vary significantly in a wide range [2, 3], making its measurement challenging. Fortunately, ultrasonic techniques have been developed and proved to be a promising solution for this task. With increasing interest, some basic principles for the measurement have been proposed [4-7]. However, some primary problems including the discontinuous measurement issue [8], the resolution issue [7], and the measurement errors [9] still exist and need to be resolved.

Sonic waves exhibit different natures when transmitting in different layers of a multi-layered structure. Therefore, different models have been developed to calculate the thickness from the reflected echoes. For a thick oil film range, the time-of-flight model [6] is used to estimate the film thickness through calculating the time taken for the echo to travel. For a thin film measurement range, overlap of the echoes is common in bearings. Two classical frequency-domain methods, namely, the resonance model [4] and the spring model [5], are effective. More specially, the resonance model is applicable when the echoes are superposed partially, in which case the correct selection of resonant frequency is essential. The spring model is suitable when the echoes are superposed completely. It is worth noting that there is a measurement gap,

namely, the blind zone, between the effective ranges of these two models. To address this issue, a newly developed method, named as phase model [10] which is capable of covering both the blind zone and the zone of the spring model, was reported.

Recently, a new model based on the principle of wave superposition was proposed to calculate the film thickness directly in the time-domain [7] and is called the referred time-domain method in this work. Without complex Fourier transformation, the reflected echoes from the oil layer can be expressed as the superposition of the transformations of the incident wave by varying the amplitude and phase [11, 12]. Then the oil film thickness of measured signals can be obtained by matching the measured signals with simulated echoes [7]. This model was reported to cover the blind zone and have a wider effective range than that of the frequency-domain models. However, there are still some ambiguities in this approach. First, the model was built with premise of identical solid materials on both sides of the oil film, and therefore is unfeasible for the exceptions. Second, the effectiveness and accuracy were not validated experimentally by comparing with the traditional models. Third, the resolution of the pre-simulated echoes relies on the sampling frequency, which may increase the sampling cost to maintain the identical resolution with the traditional methods.

In summary, there are limitations for current ultrasonic measurement of oil film thickness. For traditional frequency-domain methods, a unified and no pre-test model is required to avoid switching models for different effective ranges. In the time-domain, further work on the referred time-domain model is needed to improve its resolution and measurement capability so that an oil film thickness between two different solid materials can be measured accurately and in a wide range.

To achieve this goal, an improved time-domain method is proposed using a matching principle. Meanwhile, the optimized interpolation is applied to both simulated and measured signal for better resolution. To verify the wider measurement range, the improved time-domain method was compared with previous traditional frequency-domain and time-domain methods in a precision calibration rig.

The remainder of this paper consists of 4 sections. Section 2 mainly presents the development of new improved-domain model. It is followed by the comparison and selection

of the interpolation method by using simulation to improve the resolution issue in section 3. The experiment validation and results are reported in section 4. Computational costs of different models are compared and discussed in section 5. Finally, section 6 draws the conclusions of this work.

2. General time-domain model based on the principle of wave superposition

Different to the frequency-domain models mentioned above, the time-domain model deals with the echo waves directly based on the principle of wave superposition [11]. For an illustration purpose, a typical three-layer structure, eg, a sandwich composed by the solid-oil-solid interfaces, is used as shown in Figure 1. An incident wave I hits the first solid-fluid interface and then separates into two parts: reflected wave and transmitted wave, denoted as S and A, respectively.

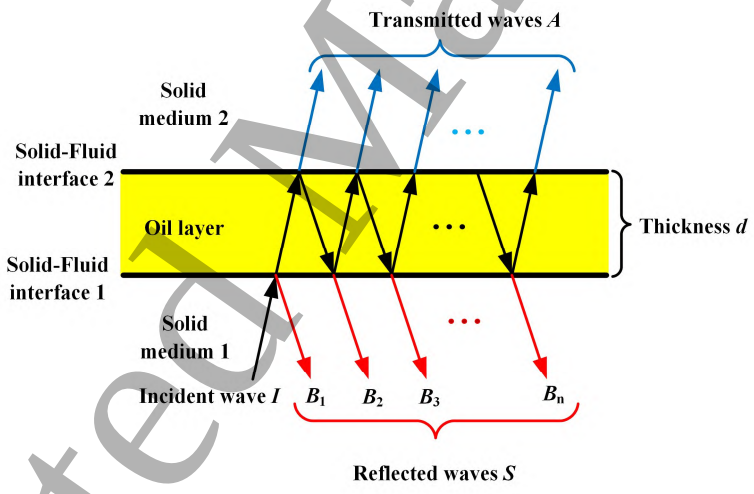

Figure 1 The principle of wave superposition of ultrasonic wave in a three-layered structure

It can be seen from Fig. 1 that the reflected waves collected at time t is $\boldsymbol{S}(t) = \{B_1(t), B_2(t), \cdots, B_n(t)\}$. Figure 2 shows the superposition phenomenon of the reflected waves $\boldsymbol{S}(t)$. For thick oil layer, the flight time of an ultrasonic wave in the oil layer is long and the corresponding collected reflected waves $\boldsymbol{S}(t)$ is separated in the time domain as illustrated in Figure 2(a). As the oil film thickness decreases, the flight time of an ultrasonic wave becomes short and partial superposition occurs between the reflected waves (Figure 2(b)). For a very thin oil layer, the

superposition degree of the reflected waves $\boldsymbol{S}(t)$ becomes severe and only a "single" reflected wave can be observed in the time domain (Figure 2(c)).

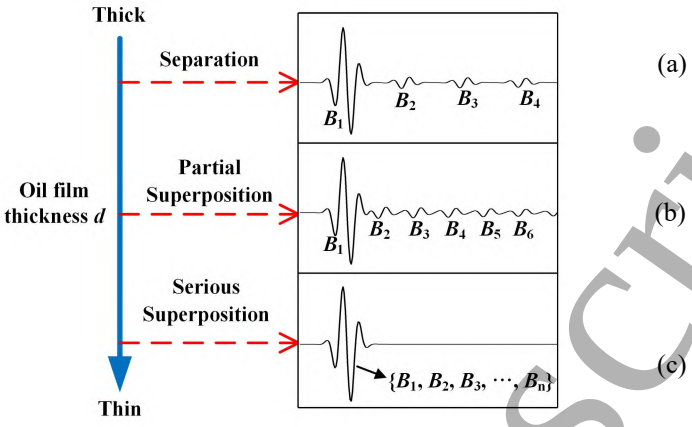

Figure 2 The superposition phenomenon of reflected waves $\boldsymbol{S}(t)$ from thick oil film to thin oil film in the time domain

Neglecting the energy dissipation, If the displacement is used to describe the transmit properties the ultrasonic wave, the assignment of the reflection and transmission waves can be represented as:

$$V_{ij}=\frac{Z_j-Z_i}{Z_j+Z_i},\quad W_{ij}=1+V_{ij} \tag{1}$$

Where V_{ij} and W_{ij} denote the displacement reflection and transmission coefficient of the incident wave from the i-th medium into the j-th one, respectively; Z ($Z=\rho c$) is the acoustic impedance of the media (given by the product of density (ρ) and speed of sound (c)).

Considering both the time lag and the amplitude variation caused by the reflection and transmission, the obtained reflected waves from the incident wave can be presented as [8]

$$\begin{aligned}
&B_1(t)=V_{12}I(t)\\
&B_2(t)=W_{12}V_{23}W_{21}I(t-T)\\
&B_3(t)=W_{12}V_{23}W_{21}(V_{21}V_{23})^1 I(t-2T)\\
&\cdots\\
&B_n(t)=W_{12}V_{23}W_{21}(V_{21}V_{23})^{n-2} I(t-(n-1)T)
\end{aligned} \tag{2}$$

Where n is the number of the reflected waves, T is the flight time of ultrasonic wave between two interfaces. Correspondingly, the overall reflected wave $S(t)$ can be obtained theoretically by superposing the reflected waves $\{B_1(t), B_2(t), \cdots, B_n(t)\}$.

The oil film thickness d can be determined by multiplying the flight time T and the sound

speed (c_2) between two solid surfaces (i.e., in the fluid medium as illustrated in Figure 1).

$$d=\frac{Tc_2}{2} \tag{3}$$

In practice, the reflection and transmission coefficient, V_{ij} and W_{ij}, can be calculated theoretically using Eq. (1). In a typical bearing structure like a solid-oil-solid structure shown in Figure 1, the ultrasonic wave would pass through these three layers with partial reflection and transmission. Therefore, it is impossible to capture the Incident signal directly. On the other hand, the amplitude and phase of the reflection coefficient of the incident wave at a solid-air interface are close to 1 and 0, respectively. Thus, it is safe to assume that the reflected signal at the solid-air interface is equal to the incident wave and can be used as the reference signal I(t). Correspondingly, the solid-air interface is regarded as the reference interface. In practice, the reference signal (i.e., reflected signal) is measured after removing the oil layer [13].

The reference signal $I(t)$ is a continuous pulse signal with the sampling interval T_s. Therefore, the overall reflected signal, $S_i(t)$, can be reconstructed theoretically using the time lag (0, i, 2i, …(n-1)i sample intervals) and the reflection and transmission induced energy loss and the reflection and transmission induced energy loss of the reference signal $I(t)$. $S_i(t)$ is presented in Eq. (4).

$$\begin{aligned} S_i(t) &= V_{12}I(t) + W_{12}V_{23}W_{21}I(t\text{-}iT_s) \\ &+\cdots+ W_{12}V_{23}W_{21}(V_{21}V_{23})^{\text{n-2}}I(t-(n-1)iT_s) \end{aligned} \tag{4}$$

Conversely, with Eq. (3) and Eq. (4), the $S_i(t)$ can be theoretically constructed with a definite oil film d_i, which can be expressed by

$$d_i=\frac{iT_sc_2}{2} \tag{5}$$

When variable i (i=1, 2, 3, …) is different, the definite oil film thickness d_i will be different. In practice, a set of $S_i(t)$ under the variable of i would be calculated to correspond with a series of thicknesses values. Then the measured signal is matched one by one to find the most approximated $S_i(t)$ and the corresponding thickness is adopted as the objective value. The matching result can be assured with the linear correlation analysis.

This so-called wave superposition is more general than that the reported one [7] because this model denotes different materials on both sides of the sandwich as seen in Fig. 1. Thus, it

is suitable for measuring an oil film thickness sandwiched between two different solid materials. In addition, it can be drawn from the reported method that the resolution of film thickness d_{min} depends on the sound velocity c_2 and sampling interval T_s (see Figure 16 in [7]). According to literature [7] and Eq. (5), when the ultrasonic wave c_2 is 1467 m/s in oil and the sampling interval T_s is 10 ns for a 100 MHz sampling system, the resolution of the film thickness measurement is 7.335 μm theoretically. The low resolution will lead to poor online measurement precision, especially when the film thickness varies in a wide range and quickly during start-stop phase of machine [2, 3]. More importantly, this issue becomes severe for thin film measurement under elastohydrodynamic lubrication because the film thickness is usually sub-micron in this case. One of the direct ways to solve this problem is using a sampling system with a much higher frequency, but this approach increases the cost. Therefore, its poor measurement resolution makes it inferior to other frequency-domain methods and become a main bottleneck for practical application.

However, the ultrasonic pulse signal has limited bandwidth, which means the ultrasonic reflected signal can be reconstructed theoretically if the sampling frequency meets the Nyquist criteria according to the "Shannon's sampling theorem" [14]. In other words, the measurement resolution is not dependent on the sampling frequency of sampling system and the sound velocity. The poor resolution issue can be resolved by using the resample and interpolation of the signal.

3. Interpolation-based improvement on the time-domain method

As mentioned in the section above, the resample and interpolation of the signal can be used to improve the resolution. Therefore, it is necessary to analyze and select an interpolation method with high precision to employ in the ultrasonic signal. The interpolation of the sampled signal can be achieved by [14,15]:

$$x(kT_s/M) = v(kT_s/M) * h(kT_s/M) \tag{6}$$

Where $x(kT_s/M)$ is the sampled signal $x(kT_s)$ with increasing the sampling rate by a factor

M; $v(kT_s/M)$ is obtained by filling in with M-1 zero-valued samples between each pair of sampled signal $x(kT_s)$. The kernel function $h(kT_s/M)$ is a digital low-pass filter.

It can be seen from Eq. (6) that the reconstruction of a sampled signal is achieved through the convolution of the signal $v(kT_s/M)$ and impulse response of a low-pass reconstruction filter in the time domain. This process can be better understood in the frequency domain. When the sampled signal $x(kT_s)$ is filled in with M-1 zero-valued samples between each pair points, the sampling rate will increase M times. The spectrum of the signal $v(kT_s/M)$ contains not only the baseband frequencies of interest (i.e., $-\pi/M$ to π/M) but also signals of the baseband centered at harmonics of the original sampling frequency $\pm 2\pi/M$, $\pm 4\pi/M$, ···. Then the digital low-pass filter $h(kT_s/M)$ is used to extract the baseband signal of the interest and eliminate the unwanted higher frequency components.

The ideal low-pass filter for reconstruction has the impulse response of a sinc function, which provides perfect interpolation for bandlimited signals with infinite length of data record. However, when the ideal low-pass filter is applied in practice, a direct truncation of the impulse response of the sinc function (i.e., a rectangular windowing of the impulse response) is necessary because the data record has only a finite length, which leads to the Gibbs' phenomenon [16]. Therefore, we need to select the interpolation method whose frequency-domain response approximates that of the ideal low-pass filter the most.

To select an appropriate interpolation method to interpolate the ultrasonic incident signal emitted by the ultrasonic transducer used in this work, the following steps were taken.

First, the Gaussian echo model was applied to simulate the incident signal emitted from the ultrasonic transducer used in this work. The Gaussian echo can be expressed as [17, 18]

$$I(\theta,t) = \beta e^{-\alpha(t-\tau)^2} cos(2\pi f_c(t-\tau)+\phi)\,, \quad \theta = [\alpha,\tau,f_c,\phi,\beta] \tag{7}$$

where θ is parameter vector, α is bandwidth factor, τ is arrival time, f_c is center frequency, ϕ is phase, and β is amplitude.

Figure 3 shows the time-domain (a) and frequency-domain (b) plot of the Gaussian echo model at $\theta = [\alpha, \tau, f_c, \phi, \beta] = [92.4, 0.4, 6.8, 4.5, -2091]$, in which the values are estimated by fitting the Gaussian echo model to the reflected signal from a steel-air interface and obtained using a ultrasound transducer with a center frequency of 6.8 MHz.

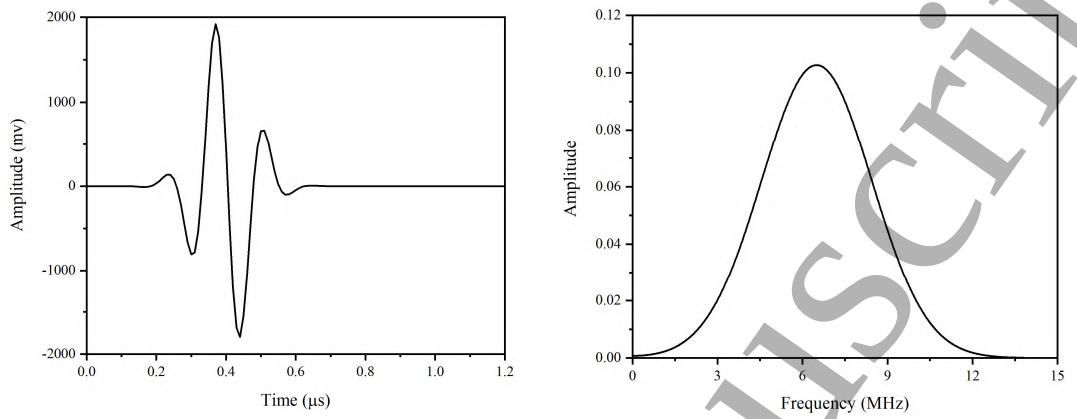

(a) (b)

Figure 3 The time-domain (a) and frequency-domain plot (b) of the Gaussian echo model when $\theta=[92.4,0.4,6.8,4.5,-2091]$

Second, the frequency-domain responses of 4 commonly used interpolation methods [14, 19-21], including linear interpolation, cubic spline interpolation, truncated sinc interpolation, and windowed sinc interpolation were obtained and plotted as shown in Figure 4. The amplitudes are normalized for the convenience of analysis. The ideal low-pass filter represents the frequency-domain response of a 'perfect' interpolation method (interpolation error is 0). The frequency-domain response of the simulated ultrasonic signal in Figure 3 (b) is re-plotted in black dash line froe easy analysis.

Third, according to Eq. (6), the frequency-domain distributions of the ultrasonic signal before and after interpolation should be the same or as close as possible to avoid spectral distortion or lowest interpolation. Therefore, the 3rd step was to select a suitable interpolation method whose response approximates the ideal low-pass filter (the red, dotted line) most.

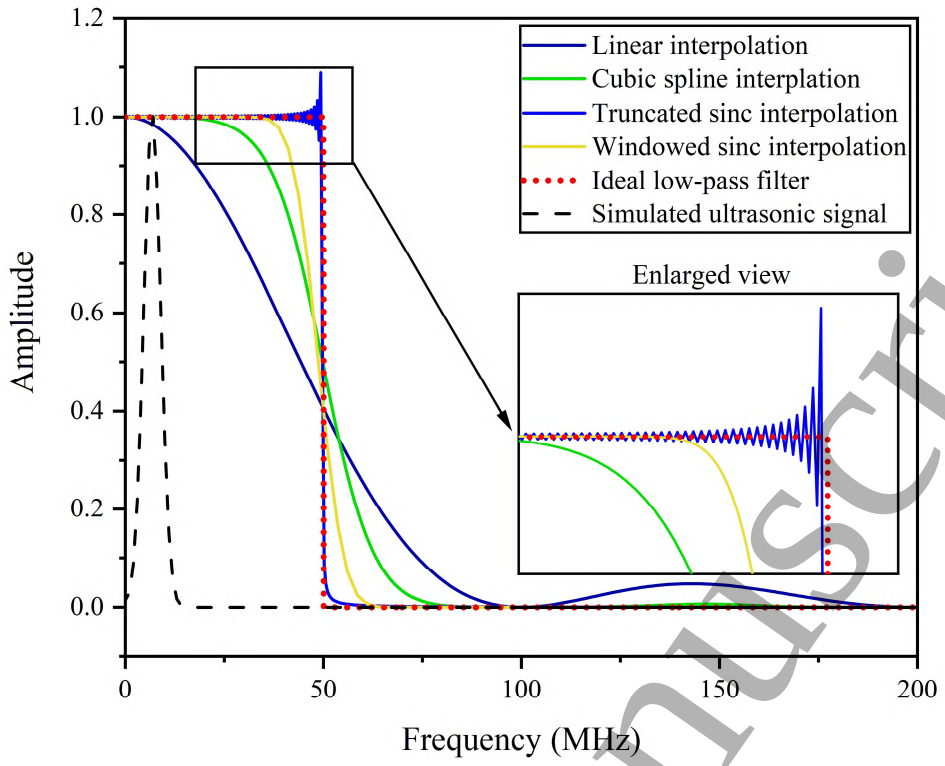

Figure 4 The frequency response of different interpolation methods, the ideal low-pass filter is plotted in red dotted line to represent the frequency-domain response of a 'perfect' interpolation method, the frequency-domain response of simulated ultrasonic signal (Figure 3 (b)) is re-plotted in dark dash line for easy analysis

As a result, it can be seen that the response of the truncated sinc interpolation seems to approximate that of the ideal low-pass filter the most but suffers the Gibbs phenomenon, that is, manifesting itself as a large ripple ((9 percent)) in the frequency behavior of the filter in the vicinity of filter magnitude discontinues as shown in the enlarged view of Figure 4. In order to eliminate or minimize this effect, one commonly used and effective way is using other windows such as Hamming windows and the Kaiser windows to truncate the impulse response of the sinc function instead of rectangular window [14]. When the Kaiser window is used to truncate the impulse of sinc function, the ripple phenomenon is reduced to a certain degree as shown in the enlarged view of Figure 4. Considering the processing times and the frequency responses using that of the ideal low-pass filter as the benchmark, the windowed sinc interpolation method was selected in this study.

Furthermore, by interpolating the ultrasonic simulated signal (Figure 3a), interpolation errors of these 4 different interpolation methods can be obtained as shown in the Table 1. The interpolation error can is calculated using

$$The\ Interpolation\ error = \frac{1}{N}\sum_{k=1}^{N}\left(I\left(\frac{kT_s}{M}\right) - \hat{I}\left(\frac{kT_s}{M}\right)\right)^2 \quad (8)$$

where $I(kT_s/M)$ is the actual value of the simulated ultrasonic signal at sampling points kT_s/M calculated using Eq. (7); $\hat{I}(kT_s/M)$ is the estimated value of the simulated ultrasonic signal at sampling points kT_s/M and using the interpolation method; N is the total sampling points of the simulated ultrasonic signal after interpolation

Table 1 The interpolation error comparison of the 4 interpolation methods

Interpolation methods	Linear interpolation	Cubic spline interpolation	Truncated sinc interpolation	Windowed sinc interpolation
Interpolation error	9.26	0.05	5.45×10^{-6}	4.19×10^{-6}

It can be seen from the Table 1 that the interpolation error of the windowed sinc interpolation method is the lowest, which is consistent with analysis about Figure 4.

Based on the analysis mentioned above, the windowed sinc interpolation is used in this work in order to avoid the effect of interpolation error on the time-domain method to the maximum degree.

Supposing that M-1 points are equally interpolated between two sample points,, the sample frequency, f_s, will be affected by the interpolation with the f_s increasing to Mf_s. Thus, the measurement resolution of the film thickness can be improved to $1/M$. In this work, the sampling frequency of PCI digitizer card is 100 MHz and 99 points are selected to interpolate in the interval between two sample points. The sampling interval T_s becomes 0.1 ns theoretically without interpolation error. The corresponding resolution of the film thickness measurement is improved to 0.0734 μm theoretically when using the sound speed of 1467 m/s in the oil layer according to Eq. (5).

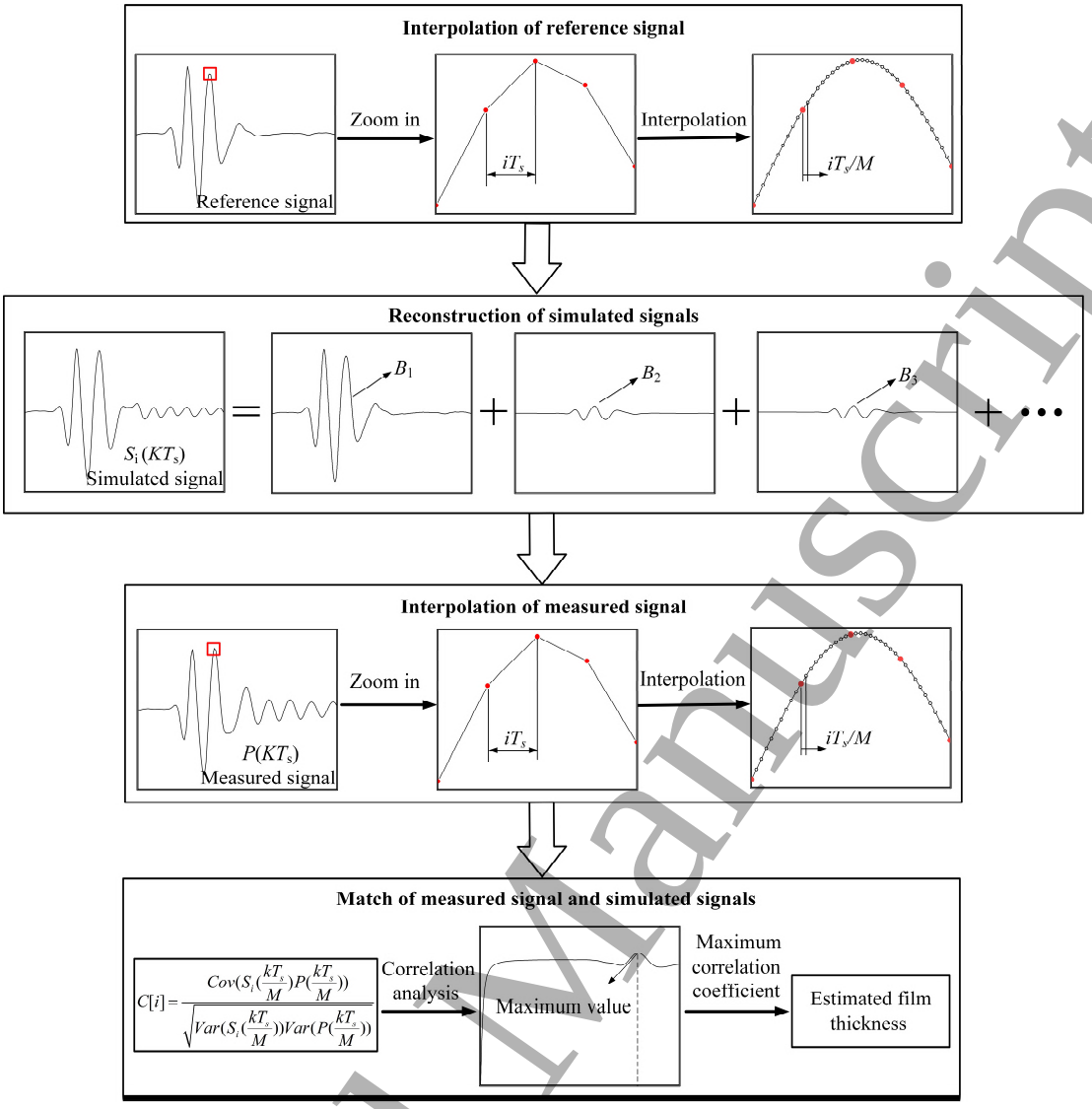

Figure 5 The signal processing procedures of the improved time-domain method

The procedures of the improved time-domain method shown in Figure 5 are described as follows.

Step 1: Interpolation of the reference signal

The reference signal from the steel-air interface $I(kT_s)$ is acquired and windowed sinc interpolation algorithm is applied to interpolate the reference signal.

Step 2: Reconstruction of simulated signals

The simulated signals from oil films of a series of thicknesses $S_i(kT_s/M)$ are reconstructed using the reference signal after interpolation $I(kT_s/M)$ and according to Eq. (4).

Step 3: Interpolation of a measured signal

The measured signal from the real oil layer $P(kT_s)$ is acquired and interpolated using the windowed sinc interpolation

Step 4: Match of the measured and simulated signals

The measured signals after interpolation $P(kT_s/M)$ are matched with the simulated signals $S_i(kT_s/M)$ one by one. The corresponding linear correlation coefficient is calculated by [22]

$$C[i]=\frac{Cov(S_i(\frac{kT_s}{M})P(\frac{kT_s}{M}))}{\sqrt{Var(S_i(\frac{kT_s}{M}))Var(P(\frac{kT_s}{M}))}} \quad (9)$$

Where $Cov()$ is covariance function and $Var()$ is variance function.

Then, the estimated film thickness with a maximum correlation coefficient is selected as the final value.

The improved time-domain method has a better resolution in comparison to the existing time-domain method and covers a full range theoretically when compared to the traditional methods (i.e., spring model, resonance model and phase model). Detailed comparisons of the improved method to the existing ones will be made in the next section.

4. Experiment and verification

4.1 Experimental setup and procedures

To demonstrate the effectiveness of the improved method, oil film thickness values, in a range of close to zero to 600 μm, were experimentally obtained using the calibration rig, whose details can be found in literature [10, 12]. The calibration rig can be used to construct oil films in different thicknesses by using a coarse adjustment component (with a movement range of 0-18 mm and a resolution of 10 μm) and a fine adjustment component (with a movement range of 0-120 μm and a resolution of 2 nm).

In this work, the piezoelectric element with a center frequency of 6.8 MHz and -12 dB bandwidth of 4~10.6 MHz was bonded to the back face of the stationary steel disk (refer to [10]). The pulser-receiver used in this work was purchased from Tribosonics Ltd, England. The excitation pulse is a negative square wave with an amplitude of 20V and a pulse width of 170

ns. The reflected signal was amplified (the gain is 5dB). The sampling frequency of the ultrasonic measurement is 100 MHz and its corresponding sampling interval is 10 ns. The properties of materials used in this work are given in Table 2.

Table 2 Material properties

Material	Density, $\rho\left(kg\cdot m^{-3}\right)$	Speed of sound, $c\left(m\cdot s^{-1}\right)$	Acoustic impedance $z\left(10^{6}kg\cdot m^{-2}\cdot s^{-1}\right)$
Oil	886	1467	1.3
Steel	5818	7810	45.4

To compare the performance of the improved model to that of the spring model, the actual film thicknesses were set between 0-20 μm using a step size 1.5 μm of the fine adjustment part. To compare the performance to that of the resonance model in a wide range, a set of the film thickness between 0-600 μm were obtained by using the coarse adjustment part with a step size of 20 μm. To compare the performance to that of the phase model, a set of the film thicknesses in the range of 0-100 μm were obtained by using the fine adjustment part with a step size of 5 μm. To evaluate the accuracy of the improved method, the film thicknesses were obtained with a fine step size of 1.5 μm in two film ranges, that is, 100-120 μm and 0-20 μm.

4.2 Experimental results

The ultrasonic signals collected at the known film thickness values (called actual film thickness in the rest of this paper) were used to estimate film thicknesses using 5 approaches, that is, the spring model [5], the resonance model [5], the phase model [10], the referred time-domain model [7] and the improved time-domain model proposed in this paper. Comparisons of these approaches and evaluations of the development presented in section 4 are divided into two parts. The first part is to verify the measurement range of the film thickness of the proposed method through comparing with the traditional spring, resonance and phase models in their measurement ranges. The second part is to demonstrate the superior performance of the interpolation based the time-domain model to the referred time-domain approach. Since the

actual film thickness values were generated from thick to thin, the comparisons were conducted and are presented below following the same sequence.

4.2.1 The comparison of the improved time-domain model and traditional models

Figure 6 shows the comparisons of the improved model with the spring model. It can be seen from the figure that the spring model is the most accurate when the film thickness is less than 7.5 μm, evidenced by $|R|<0.95$, where $|R|$ is the reflection coefficient amplitude of oil layer [5]. In a range of 7.5 – 17 μm, the film thicknesses estimated using the spring model have a large error and large deviations to the actual values with $|R|>0.95$. In comparison, the improved time-domain method overall performs well in this range. It has a relatively larger error in the very thin film region (< about 2 μm), which will be discussed in section 4.2.3.

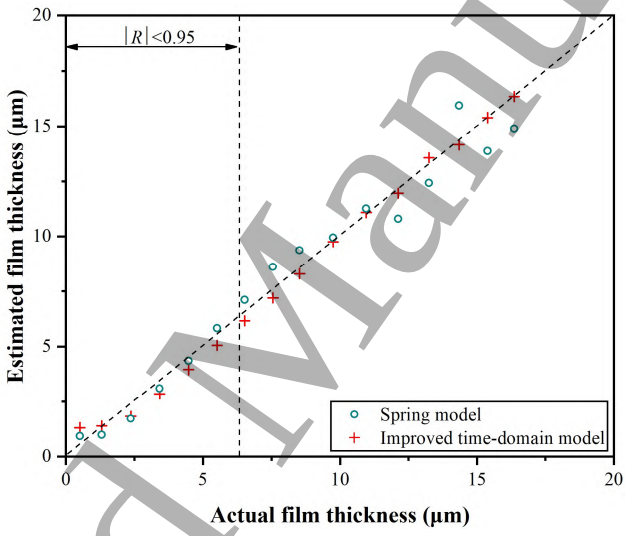

Figure 6 The quantitative comparisons of the improved time-domain model and the spring model

Figure 7 shows the comparisons of the improved model with the resonance model. It can be seen from figure that the measurement results of the improved time-domain method are highly consistent with those of the film resonance method in the measurement range of the resonance model. The advantage of this improved approach over the resonance method is presented below.

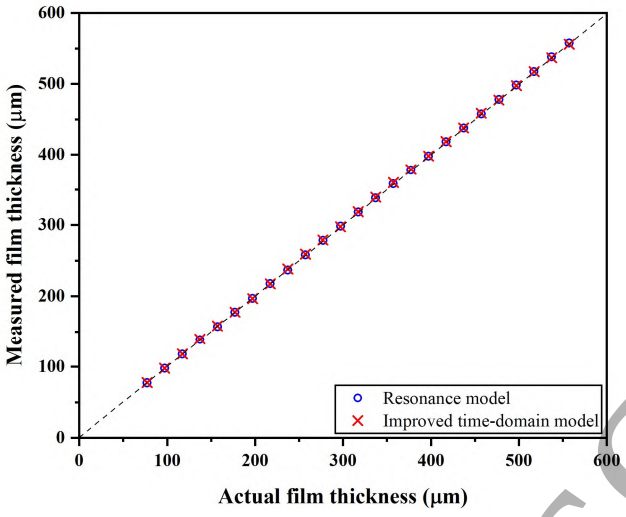

Figure 7 The comparison of the performance of the resonance model and the improved time-domain model in a film thickness of 80 – 600 μm

Previous studies demonstrate that the selection of a correct mode can be a significant issue when applying the resonance model especially for the transducer with a narrow bandwidth [9]. If multiple minima are present, then the mode number can be determined by using the interval of neighboring resonant frequencies, after which the film thickness can be calculated by film resonance equation [10]. However, if only one resonant minimum exists within the bandwidth, the mode number needs to be assumed before calculating the film thickness. It can be seen from Figure 8(a) and 8(b) that only one minimum can be observed in the -12dB bandwidth for the reflected signal from oil films at 107.24 μm and 207.24 μm. In this case, the mode of resonant frequency cannot be determined only by this single signal.

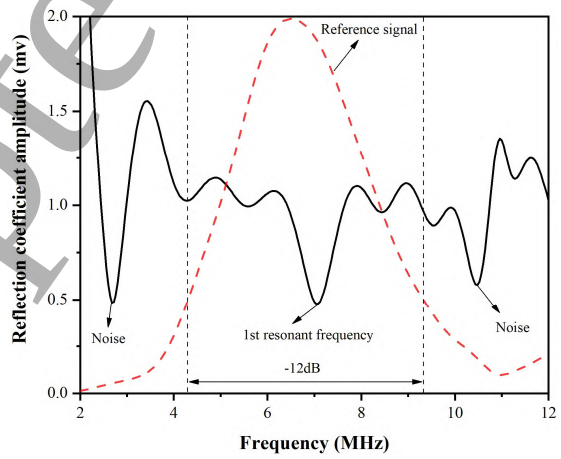

(a)

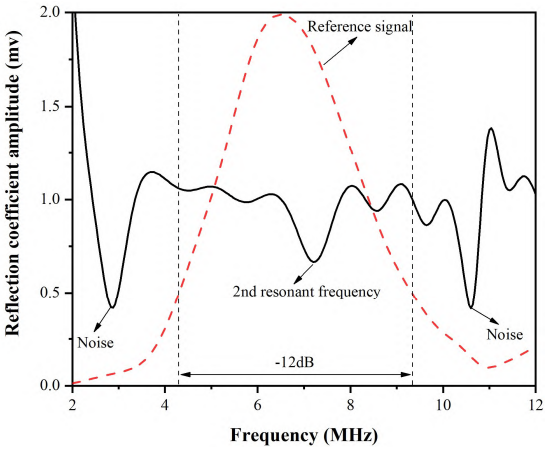

(b)

Figure 8 The frequency-domain plot of reflected signal from oil layers at (a) 107.24 μm and (b) 207.24 μm

In comparison, the improved time-domain model is based on the matching of the measured signal with the simulated signal, which means that the film thickness can be calculated without the mode assumption. Figure 9 shows the matched results using this method for the actual oil film thicknesses of 107.24 μm and 207.24 μm. The results are 108.78 μm and 207.73 μm, respectively. Therefore, the improved time-domain model is superior to the resonance model based on this point.

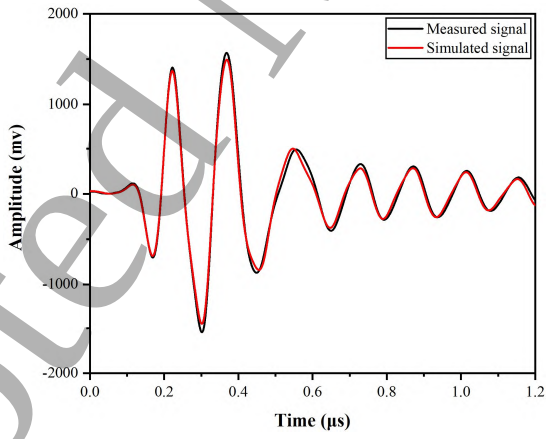

(a)

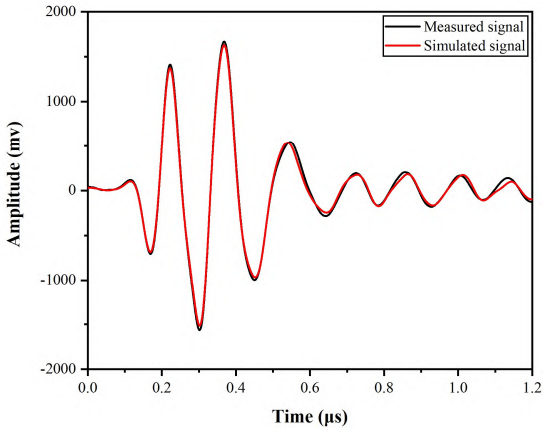

(b)

Figure 9 Comparisons of the measured signal and matched simulated signals using the proposed approach at an oil film thickness of 107.24 μm (a) and 207.24 μm (b), respectively

Figure 10 shows the performance of the improved time-domain model vs that of the spring model, the resonance model and the phase model. In the blind zone (5-58 μm) where the resonance model and spring model are invalid [10], the film thicknesses estimated using the improved time-domain method agree well with the real film thickness values. Therefore, these results demonstrate that the same as the phase model, improved time-domain method with interpolation can also produce more reliable film thickness estimation in the blind zone and have wider measurement range than phase model.

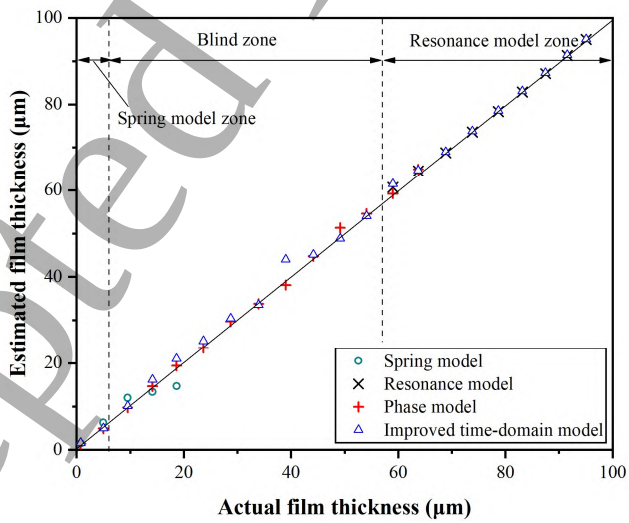

Figure 10 The comparison of the performance of the traditional models and the improved time-domain model in the film thickness of 0 – 100 μm

To summarize, the above experiments show that the improved time-domain model is a

unified method, which can cover the range of all the traditional models.

4.2.2 The comparison of the improved time-domain method and existing time-domain method

Figure 11 shows the comparison to the referred time-domain model [7] in 100-120 μm and 0-20 μm. The film thickness estimation in the blind zone will be presented and discussed in section 4.2.3.

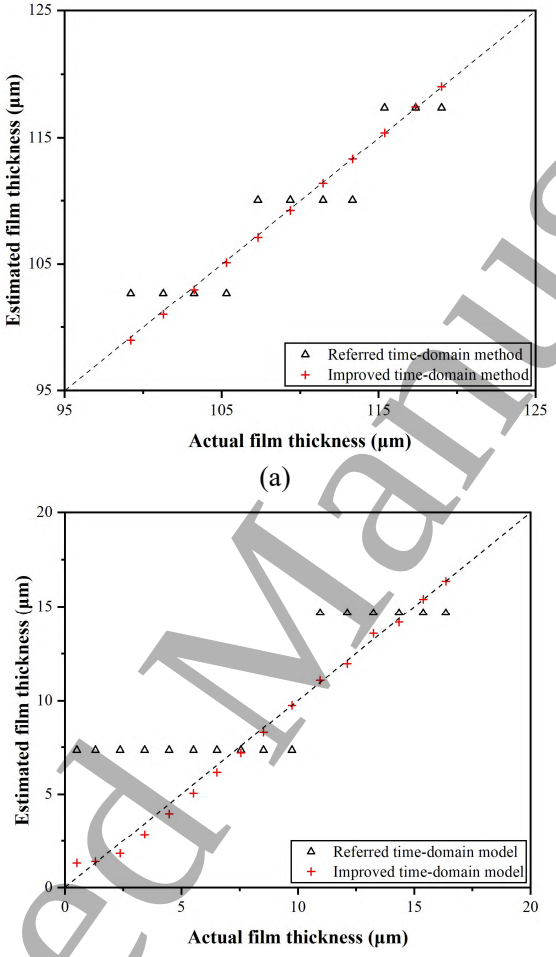

Figure 11 Comparison of oil film thicknesses calculated using the referred time-domain model and the improved model to the experimentally measured values. (a) thick oil films, (b) thin oil films

It can be seen that the data from the referred time-domain model is grouped into horizontal lines, deviating from the 45 diagonal line (i.e., the actual film thickness values) seriously. This is because the measurement resolution of the referred time-domain model is only 7.335 μm theoretically. In comparison, the improved model is highly consistent with the actual film thickness thanks to the theoretical measurement resolution of 0.07335 μm. In addition, the

referred time-domain model is inferior to the improved method for thin films (Figure 11 (b)). The results demonstrated that the improved time-domain approach with interpolation improves the measurement resolution and accuracy of film thickness.

4.2.3 The overall comparison of different models

In addition to the above comparisons, the relative errors (in percent) of the calculated film thickness to the actual film thickness in the film thickness range of 0-100 μm were quantified. Five repeated measurements were conducted for each film thickness. The averaged values are now reported in Table 3.

In the oil film thickness range of 58-95 μm (i.e., the resonance model zone), resonance model, time-domain and improved time-domain models produce very similar results with an error within 5%. Compared with the improved model, the referred time-domain model has evidently higher error, except at the film thickness of 59 μm. In the blind zone (5-58 μm), the percentage errors of the improved time-domain model and phase model are similar and globally lower than those of the existing methods. In the spring model zone (0-5 μm), the improved time-domain model has a lower error compared to the other model. In summary, both the current and improved time-domain models cover a wider range than the traditional models do. In comparison of these two time-domain models, the improved model offers higher accuracy. In summary, the improved time-domain model covers the measurement ranges of the frequency-domain models and has higher resolution than the referred time-domain model.

Table 3 also reveals that the measurement errors of the improved model become higher when the oil film thickness is less than about 40 μm. This may be related to the surface roughness effect (see Figure 18 in [9]). When the oil film thickness is thin (eg, < 20 μm), the reflected signal can be easily "contaminated" by error sources including electrical noise, sound waves reflected from surrounding materials, surface roughness, resulting in a relatively higher error in the measurement. Due to the asperities of the disk surface, it is very difficult to generate or control an oil film thinner than 2 μm in practice. Therefore, the relative measurement error of the improved model is the highest at the smallest oil film thickness (0.78 μm).

Table 3 The relative error (%)* comparison of the 5 models

Actual film thickness (μm)	Spring model	Resonance model	Phase model	Referred time-domain model	Improved time-domain model
95.05		0		0.32	0.12
91.52		0.23		3.82	0.01
87.49		0.41		0.61	0.15
83.15		0.33		2.96	0.16
78.67		0.46		2.56	0.12
73.83		0.30		0.65	0.03
68.86		0.15		4.13	0.13
63.76		1.18	8.40	3.54	1.40
59.01		2.84	6.90	0.56	3.82
54.10			15.47	18.65	0.21
49.16			17.75	10.47	0.54
44.17			11.42	0.36	2.40
39.01			7.79	17.26	12.93
33.97			10.32	13.63	8.91
28.75			14.13	2.06	4.35
23.67			9.06	7.03	7.04
18.66	21.80		20.68	17.94	10.08
14.14	4.01		12.05	3.76	9.68
9.53	28.56		7.31	22.81	4.70
5.00	24.11		2.50	47.15	0.09
0.78	88.35		120.67	845.13	113.02

* The relative error = |estimated film thickness – actual film thickness|/actual film thickness

5. Computational cost and discussion

To computation times of the 5 different approaches, MATLAB software and a laptop (Inter Core i7-8550U CPU @ 1.8 GHz) was used. The mean processing time was obtained by averaging ten measurement durations.

Table 4 shows the processing times of the 5 approaches in spring model zone (0-10 μm), blind zone (10-60 μm), resonance model zone (60-100 μm). For frequency-domain models (spring model, phase model and resonance model), it can be seen that in their respective effective range, the spring model is the fastest, followed by the phase model. The processing time of the resonance model is longer than that of the spring model and the phase model because the zero-paddings algorithm is used to increase the frequency resolution in order to obtain the accurate resonant frequency.

For the time-domain models (referred time-domain model and improved time-domain model), they cover the entire range of 0-100 μm. The referred time-domain model performs the best among these five models in terms of the processing time. In comparison, the improved time-domain model has the longest processing time among these five models, which is mainly caused by the extra time taken in the interpolation of measurement data and the matching process of the measured and simulated signals. However, the computational time is still in millisecond. Therefore, the improved time-domain model is still acceptable for the online measurement of sliding bearings where the oil film thickness usually varies in a range of 0~100 μm [2, 3].

If the variation of oil film thickness is in several hundred microns, the computational cost will be larger and the proposed time-domain method needs to be further developed through algorithm optimization. Alternatively, a two-step approach is suggested. A quick method (eg, the referred time-domain model in the blind or resonance model zone) is used to estimate the range coarsely. The improved time-domain model is then applied to perform fine measurement

of the film thickness in this range. This approach will save the measure time and is particularly attractive when a thin oil film needs to be measured quickly and accurately.

Table 4 Comparison of the computational times (in ms) of the existing methods and the proposed approach in three measurement zones

Oil film thickness (μm)	Spring model	Resonance model	Phase model	Referred time-domain model	Improved time-domain model
0-10 (Spring model zone)	10.85			3.90	72.62
10-60 (Blind zone)			12.83	5.84	260.49
60-100 (Resonance model zone)		53.67		4.39	214.33

6. Conclusion

To solve the choice problem of different ultrasonic models for measurement of oil film thickness in a large range, a unified time-domain approach is proposed for full range measurement for on-line purpose. The matching principle was adopted to obtain the oil film thickness of the measured signals with pre-constructed ones. Furthermore, the windowed sinc function was employed to interpolate both the measured and constructed signals simultaneously to improve the resolution. The proposed method was evaluated with a precision calibration rig and compared with previous traditional models. The main results can be as follows:

1) Compared with spring model, the improved time-domain method covers its measurement range and shows higher accuracy in thick films.

2) Compared with resonance model, the improved time-domain method is able to measure the film thickness without the assumption of mode of resonant frequency and shows highly consistent measurement result in the film resonance zone.

3) Compared with phase model, the improved time-domain method covers its measurement range and shows similar measurement result in the blind zone.

4) Compared with referred time-domain model, the improved method has higher resolution and larger measurement range.

Acknowledgments

The authors appreciate the financial support from the National Science Foundation of China (No. 51675403 and No. 51975455) and the International Collaborative Plan of Shaan'xi province (No. 2017kw-034) to this work. The support of K. C. Wang Education Foundation is also grateful.

References

[1] Etsion I and Constantinescu I 1984 Experimental observation of the dynamic behavior of noncontacting coned-face mechanical seals *TRIBOL T* **27** 263-270

[2] Glavatskih S B, McCarthy D M C and Sherrington I 2003 Further transient test results for a pivoted-pad thrust bearing *Tribol. Interface Eng.* **43** 301-312

[3] Li P, Zhu Y, Zhang Y, Chen Z and Yan Y 2013 Experimental study of the transient thermal effect and the oil film thickness of the equalizing thrust bearing in the process of start-stop with load *Proc. Inst. Mech. Eng. Part J.-J. Eng. Tribol.* **227** 26-33

[4] Haines, N. F 1978 The application of broadband ultrasonic spectroscopy to the study of layered media *J. ACOUST. SOC. AM.* **64** 1645

[5] Tattersall H G 1973 The ultrasonic pulse-echo technique as applied to adhesion testing *J. Phys. D-Appl. Phys.* **6** 819-832

[6] Dwyer-Joyce R S, Drinkwater B W and Donohoe C J 2003 The measurement of lubricant-film thickness using ultrasound *Proc. R. Soc. A-Math. Phys. Eng. Sci.* **459** 957-976

[7] Praher B and Steinbichler G Ultrasound-based measurement of liquid-layer thickness: A novel time-domain approach *Mech. Syst. Signal Proc.* **82** 166-177.

[8] Zhang J, Drinkwater B W and Dwyer-Joyce R S 2005 Calibration of the ultrasonic lubricant-film thickness measurement technique *Meas. Sci. Technol.* **16** 1784-91

[9] Hunter A, Dwyer-Joyce R S and Harper P 2012 Calibration and validation of ultrasonic reflection methods for thin-film measurement in tribology *Meas. Sci. Technol.* **23** 105605

[10] Dou P, Wu T and Luo Z 2019 Wide Range Measurement of lubricant film thickness based on ultrasonic reflection coefficient phase spectrum *ASME J. Tribol.* **141**

[11] Brekhovskikh L et al 1980 Chapter I—Plane Waves in Discretely Layered Media (*Applied Mathematics and Mechanics*, Vol.16) Elsevier New York 1–129

[12] Dou P, Wu T, Luo Z, Peng Z, and Sarkodie-Gyan T 2019 The application of the principle of wave superposition in ultrasonic measurement of lubricant film thickness *Measurement* **137** 312-322

[13] Reddyhoff T, R S Dwyer-Joyce, J Zhang and B W Drinkwater 2008 Auto-calibration of ultrasonic lubricant-film thickness measurements Meas. Sci. Technol. 19 45402.

[14] Crochiere R E and Rabiner L R Interpolation and decimation of digital signals—A tutorial review *Proc. IEEE* **69** 300-331

[15] Graham and W R 2018 Interpolation for de-Dopplerisation *J. Sound Vibr.* **422** 210-236

[16] Jenq Y C 1994 Sinc interpolation errors in finite data record length[C]// *Conference Proceedings. 10th Anniversary. IMTC/94. Advanced Technologies in I & M. 1994 IEEE Instrumentation and Measurement Technology Conference (Cat. No.94CH3424-9). IEEE*

[17] Demirli R and Saniie J 2001 Model-based estimation of ultrasonic echoes Part I: Analysis and algorithms *IEEE Trans Ultrason. Ferroelectr. Freq. Control* **48** 787-802

[18] Demirli R and Saniie J 2001 Model-based estimation of ultrasonic echoes. Part II: Nondestructive evaluation applications *IEEE Trans. Ultrason. Ferroelectr. Freq. Control* **48** 803-811

[19] Parker J A, Kenyon R V and Troxel D E 1983 Comparison of interpolating methods for image resampling *IEEE Trans. Med. Imaging.* **2** 31-39

[20] Thévenaz P, Blu T, and Unser M 2000 Interpolation revisited [medical images application] *IEEE Trans. Med. Imaging.* **19** 739-758

[21] Unser M 2000 Sampling-50 years after Shannon *Proc. IEEE* **88** 569-587

[22] Lee Rodgers J and Nicewander W A 1988 Thirteen ways to look at the correlation coefficient *Am. Stat.* **42** 59-66